





Article

In Silico and In Vitro Studies of 4-Hydroxycoumarin-Based Heterocyclic Enamines as Potential Anti-Tumor Agents

Mediha Assad ^{1,2}, Rizwan Nasir Paracha ³ , Abu Bakar Siddique ⁴ , Muhammad Ashraf Shaheen ^{4,*}, Nadeem Ahmad ⁵, Muhammad Mustaqeem ⁴, Fariha Kanwal ⁶, Muhammad Zia Ul Mustafa ⁴ , Muhammad Fayyaz ur Rehman ⁴ , Sumaya Fatima ⁷ and Changrui Lu ^{1,*}

¹ College of Biological Sciences and Medical Engineering, Donghua University, 2999 North Ren Min Road, Shanghai 201620, China

² Department of Chemistry, Government Graduate Islamia College for Women Cantt Lahore, Lahore 54000, Pakistan

³ Department of Chemistry, Thal University Bhakkar, Bhakkar 30000, Pakistan

⁴ Institute of Chemistry, University of Sargodha, Sargodha 40100, Pakistan; abubakar.siddique@uos.edu.pk (A.B.S.)

⁵ Department of Pharmacy, Comsats University Islamabad, Lahore Campus, Lahore 54000, Pakistan

⁶ School of Biomedical Engineering, Shanghai Jiaotong University, Shanghai 200030, China

⁷ Research Center, The Fourth Hospital of Hebei Medical University, Shijiazhuang 050011, China

* Correspondence: ashraf.shaheen@uos.edu.pk (M.A.S.); crlu@dhua.edu.cn (C.L.)

Abstract: The present study reports the one-step synthesis of several 3-formyl-4-hydroxycoumarin-derived enamines (**4a–4i**) in good yields (65–94%). The characterization of the synthesized compounds was carried out via advanced analytical and spectroscopic techniques, such as melting point, electron impact mass spectrometry (EI-MS), ¹H-NMR, ¹³C-NMR, elemental analysis, FTIR, and UV-Visible spectroscopy. The reaction conditions were optimized, and the maximum yield was obtained at 3–4 h of reflux of the reactants, using 2-butanol as a solvent. The potato disc tumor assay was used to assess *Agrobacterium tumefaciens*-induced tumors to evaluate the anti-tumor activities of compounds (**4a–4i**), using Vinblastine as a standard drug. The compound **4g** showed the lowest IC₅₀ value (1.12 ± 0.2), which is even better than standard Vinblastine (IC₅₀ 7.5 ± 0.6). For further insight into their drug actions, an in silico docking of the compounds was also carried out against the CDK-8 protein. The binding energy values of compounds were found to agree with the experimental results. The compounds **4g** and **4h** showed the best affinities toward protein, with a binding energy value of −6.8 kcal/mol.

Keywords: coumarin; hydroxycoumarin; enamines; anti-tumor



Citation: Assad, M.; Paracha, R.N.; Siddique, A.B.; Shaheen, M.A.; Ahmad, N.; Mustaqeem, M.; Kanwal, F.; Mustafa, M.Z.U.; Rehman, M.F.u.; Fatima, S.; et al. In Silico and In Vitro Studies of 4-Hydroxycoumarin-Based Heterocyclic Enamines as Potential Anti-Tumor Agents. *Molecules* **2023**, *28*, 5828. <https://doi.org/10.3390/molecules28155828>

Academic Editors: Beata Morak-Młodawska, Parvesh Singh and Lalitha Gummidi

Received: 20 June 2023

Revised: 20 July 2023

Accepted: 26 July 2023

Published: 2 August 2023



Copyright: © 2023 by the authors. Licensee MDPI, Basel, Switzerland. This article is an open access article distributed under the terms and conditions of the Creative Commons Attribution (CC BY) license (<https://creativecommons.org/licenses/by/4.0/>).

1. Introduction

Despite recent progress in oncology, treating tumors via chemotherapy also affects neighboring normal cells, which is still a challenge to be addressed [1]. Reports from the World Health Organization (WHO) reveal the noxious nature of cancer, which may cause more than 13 million deaths by 2030 [2]. At present, cancer is the second-leading cause of mortality (approximately 30%) in the world and will take the top position in the next few decades [3]. Therefore, the development of potent anticancer and anti-tumor agents is urgently needed.

Several drugs based on herbal formulations [4], inorganic complexes [5], and organic moieties [6] have been reported to have anti-tumor potential. These drugs can suppress or kill the abnormal cells in localized areas but have several disadvantages, such as herbal medicines having high IC₅₀ values and less selectivity, while metal-based drugs are toxic to different body parts [7,8]. Metal-based drugs may also cause genetic mutations and affect renal functions [9]. In this regard, organic compounds with versatile moieties are of great interest due to their targeted actions and low IC₅₀ values [10–12].

Among biologically active organic compounds, coumarin derivatives have attracted special attention from synthetic and medicinal chemists [13]. Coumarins, oxygen-bearing heterocycles with a benzopyrone skeleton, are naturally occurring compounds extracted from different plants, fungi, and bacteria [14]. This class of compounds has exhibited antimicrobial, antioxidant, antifibrotic, and anti-inflammatory effects [15] and anti-tumor potential. For example, fraxetin showed anti-tumor activity against hepatocellular carcinoma (HCC) cells [16]. Some commercially available coumarin-based drugs are shown in Figure 1 [17–20]. Among coumarin derivatives, enamines derived from coumarins are proven to be important compounds that can act as anti-tumor, antibacterial, antiproliferative, and antifungal agents [21,22]. Different strategies can be used to derivatize these heterocyclic compounds, but multistep synthesis routes often affect the yields of the final products. Therefore, one-step optimized reactions are always preferred to obtain good yields in shorter times [23].

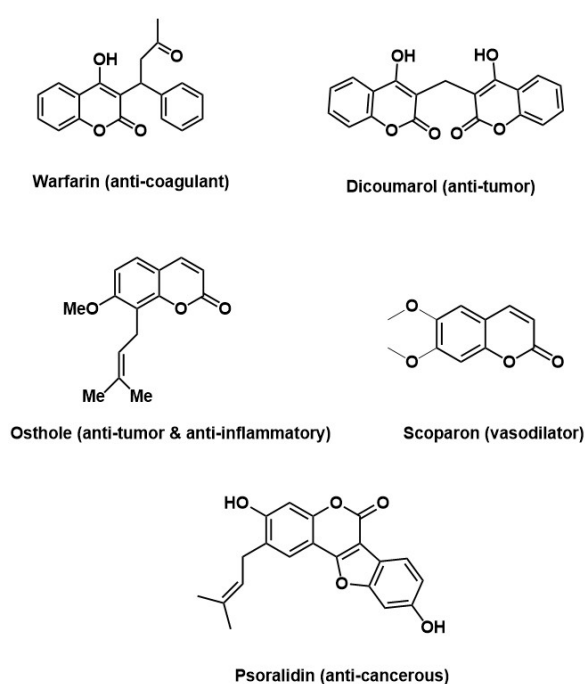


Figure 1. Commercially available coumarin-based drugs [17–20].

Although many derivatives of coumarins have been tested recently, the target selection and proper delivery of anti-tumor agents to the target area still require the development of new derivatives. The properties of coumarin derivatives can be tuned by introducing different electron-withdrawing and electron-donating groups. Therefore, the development of substituted heterocyclic enamines that can selectively pass the cell barriers of tumor cells and interact with cell proteins is an interesting area [24]. Although many cell proteins can be targeted to control cell growth, the selective targeting of the CDK-8 enzyme can be a good strategy. This enzyme plays an important role in the cell cycle, i.e., gene transcription, neuronal function, insulin secretion, and glycogen synthesis, and if a drug blocks its active site, many types of tumor growth can be controlled [25,26]. Since the effects of coumarin derivatives on the CDK-8 protein have been scarcely studied, we have targeted this protein to study the *in silico* effects of newly synthesized coumarin-based enamines.

In the present study, the synthesis of 3-formyl-4-hydroxycoumarin-derived enamines (4a–4i) is reported with good to excellent yields (65–94%). After successful characterization, the compounds were evaluated against an *Agrobacterium tumefaciens*-mediated tumor via the potato disc tumor assay. The compounds were also tested for their *in silico* binding interactions with CDK-8.

2. Results and Discussion

2.1. Characterization of Compounds (4a–4i)

One pot synthesis of 3-formyl-4-hydroxycoumarin-based enamines (4a–4i) was performed by the condensation reaction of 4-hydroxy-2*H*-chromen-2-one (1), benzyl amine derivatives (2) and triethyl orthoformate (3) under 3–4 h reflux at 80 °C. All the compounds were characterized by spectroscopic and analytical techniques, such as FT-IR, UV-Visible spectroscopy, ¹H-NMR, ¹³C-NMR, EI-MS, elemental analysis, and melting point. In FTIR spectra, the synthesis of target compounds was indicated by the absorption bands in the range of 3200–3400, 1680, and 1600 cm⁻¹, attributed to the vibrations of NH, C=O, and C=N functional groups, respectively. The appearance of the imine group peak (C=N) at 1600 cm⁻¹ was the main indication of product formation. In UV-Vis spectra, electronic transitions in the range of 19,380–19,500 cm⁻¹ were assigned to the π→π* and n→π* transitions in compounds (4a–4i). High Molar absorptivity constant values (ε = 12,350 L·mol⁻¹·cm⁻¹) were observed for π→π* transitions at lower wavelength than n→π* transitions (ε = 945 L·mol⁻¹·cm⁻¹) occurring at longer wavelength region. These transitions were in accordance with the color of purified compounds.

The ¹H-NMR spectra (Figures S1A–S9A) revealed the presence of both (*Z*) and (*E*) isomers, as shown in Figure 2. The β-hydrogen *cis*- to the cyclic ester functional group of an α,β-unsaturated ester appeared up field, hence representing the (*E*) isomer of hydroxy-enamine, while the exocyclic vinyl proton in (*Z*) isomers appeared at a higher chemical shift (δ) value. In the ¹H-NMR spectra, the signals at the lowest chemical shift (3.82–3.94 ppm) were assigned to the methoxy protons, and two signals around 4.68 and 4.72 ppm represented the methylene protons in (*E*) and (*Z*) isomers, respectively. The aromatic protons of both phenyl rings appeared in the range of 6.83–7.85 ppm. Finally, two broad signals around 10–12 ppm were assigned to NH protons of both (*Z*) and (*E*) isomers. The signal at a higher chemical shift value was assigned to the (*E*) isomer because of strong intramolecular H-bonding between H(17) and O(11), while the signal at the lower chemical shift value was assigned to the (*Z*) isomer due to weak H-bonding between O(12) and H(17) [27,28]. The intensity of the (15) signal around 8.5–8.8 ppm due to (*E*) and (*Z*) isomers indicated the presence of the (*E*) isomer in a higher ratio (72%) than the (*Z*) isomer (28%), and this was attributed to the extra-stability of (*E*) isomer due to strong H-bonding.

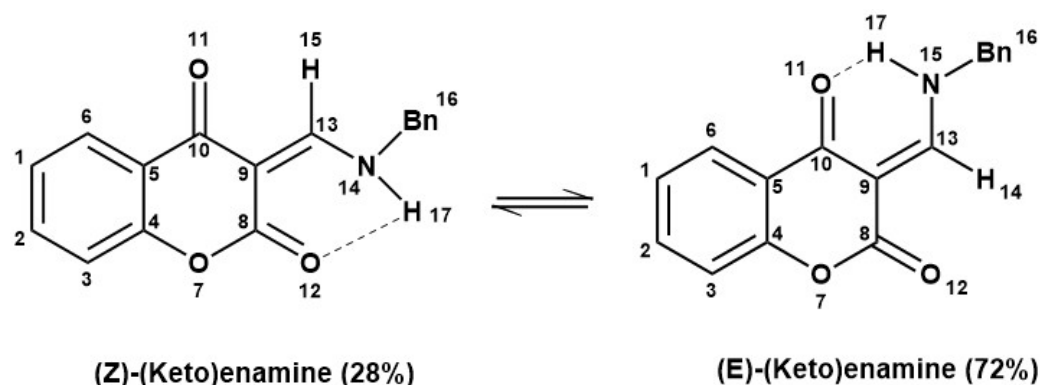


Figure 2. Tautomerism of (*E*)-(Keto)enamine and (*Z*)-(Keto)enamine.

The ¹³C-NMR spectra (Figures S1B–S9B) decoupled with (¹³C-¹H/¹³C-¹⁹F) signals showed the chemical shift value for each carbon atom of the designed compound. The coupling constant values of (¹³C-¹H/¹³C-¹⁹F) coupling are very high, in the range of 200–300 Hz. Therefore, the decoupling of (¹³C-¹H/¹³C-¹⁹F) signals was carried out to avoid the peak broadening and accurate determination of chemical shift values. The signals at chemical shift values of 50–55 ppm, 110–150 ppm, and 160–165 ppm were assigned to the carbons of methylene, aromatic ring, and carbonyl groups, respectively. Elemental analysis of the compounds was carried out to check the elemental composition and purity.

The percentages of elements (C, H, and N) were found in agreement with the calculated values, indicating the purity and the formation of desired compounds. Moreover, m/z value molecular ion peaks in the EI-MS spectrum were also found in accordance with the predicted molecular mass of compounds.

2.2. Optimization of Reaction Conditions

Several catalysts, including acids, bases, and metal salts, were screened to observe their effect on reaction yield and time, as shown in Table 1. Among these solvents, 2-butanol was the best choice with respect to the product yield. Neutral conditions of the reaction were found to be the most suitable for the product yield. Moreover, no effect was observed on the isomeric forms of the compound. Both isomers (E and Z forms) were found in the reaction mixture, with and without a catalyst.

Table 1. Optimization of reaction conditions of enamine synthesis.

Sr. No.	Solvents	Catalysts	Reaction Conditions	Yield %
1	MeOH	-	Reflux, 3 h	80
2	EtOH	-	Reflux, 3 h	75
3	THF	-	Reflux, 3 h	65
4	CHCl ₃	-	Reflux, 3 h	64
5	2-BuOH	-	Reflux, 3 h	94
6	2-BuOH	-	Reflux, 6 h	78
7	2-BuOH	AcOH	Reflux, 3 h	55
8	2-BuOH	ZnCl ₂	Reflux, 3 h	72
9	2-BuOH	AlCl ₃	Reflux, 3 h	74
10	2-BuOH	(CH ₃ COO) ₂ Pb	Reflux, 3 h	71
11	2-BuOH	Net ₃	Reflux, 3 h	60
12	2-BuOH	HCl	Reflux, 3 h	52

2.3. Anti-Tumor Activity

The anti-tumor activity of compounds (**4a–4i**) was performed following the potato disc tumor assay [29]. Potato disc tumor assay is a rapid, reliable, and preliminary method to evaluate the anti-tumor potential of compounds in laboratories. This assay is used to evaluate the anti-mitotic potential of compounds to control tumor growth. *A. tumefaciens*-induced tumor is a common disease in plants [30]. These bacteria contain tumor-inducing plasmids, which cause uncontrolled cell growth in plants, and large sized tumors appear on their surfaces. The histology and nucleic acid have shown the close similarity of these tumors to human cancer cells. Therefore, this test was performed to evaluate the anti-tumor potential of compounds [31,32].

Interestingly, it was observed that compounds (**4a**, **4c**, **4e**, **4g**, and **4h**) have better anti-tumor activities than the standard drug Vinblastine. Of these compounds, **4g** showed the strongest cytotoxic activity with $IC_{50} = 1.12 \pm 0.02$ mg/mL, while other compounds **4b**, **4d**, **4f**, and **4i** were observed to show moderate potency with IC_{50} values between 22.7–37.1 mg/mL, as shown in Table S1. A comparison of the IC_{50} values of compounds has been depicted in Figure 3.

2.4. Molecular Docking Studies

Probing in silico interactions of synthetic drug candidates with the targeted proteins or biomolecules is an effective strategy to evaluate their efficacy and mode of action [33,34]. Cyclin dependent kinases (CDKs) are actively involved in the cell cycle and other cellular phenomena, including gene transcription, neuronal function, insulin secretion, and glycogen synthesis. CDKs inhibitors are extensively studied in cancer therapy because these agents can block the cell cycle and control cell proliferation by inhibiting the CDK

enzyme activity [35]. CDK-8 is an important enzyme that plays the main role in the cell cycle; therefore, this enzyme is targeted for the in silico studies of compounds [36].

Docking interactions with CDK-8 revealed the good binding energies of all the compounds. The docking score of each compound with CDK-8 is given in Table 2. Among all the compounds, **4g** and **4h** exhibited the best binding score, consistent with the experimental studies (Figure 4). Both types of interactions (H-bonding and hydrophobic interactions) were observed between compounds and CDK-8. Amino groups of Tyr-99, Glu-101, His-154, Gly-161, and Phe-195 were involved in the H-bonding with the oxygen atoms of ligands, while hydrophobic interactions were observed between Phe-5, Lys-47, Asp-98, Tyr-153, and Tyr-156 residues and carbon atoms of ligands. In addition to synthesized compounds, the docking simulations of vinblastine and native protein-bound ligand, i.e., 8-(3-(3-amino-1*H*-indazol-6-yl)-5-chloropyridin-4-yl)-2,8-diazaspiro[4.5]decan-1-one (5XG) were performed with the CDK-8. Vinblastine and 5XG exhibited good binding scores of -9.11 and -9.18 kcal/mol, respectively. However, **4a**, **4c**, **4e**, **4g**, and **4h** bind better with CDK-8 than vinblastine and native ligand, 5XG. These interactions showed that the protein-ligand complexes are highly stable. Docking simulations of compounds (**4a**, **4b**, **4c**, **4d**, **4e**, **4f**, **4i**, and vinblastine) are presented in Figure S10.

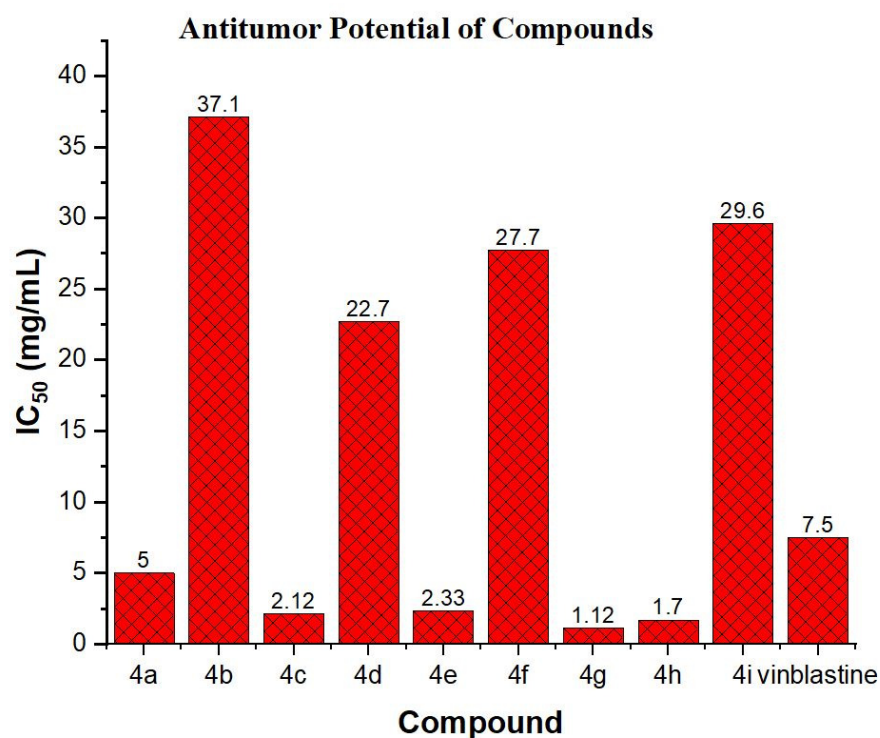


Figure 3. IC₅₀ values of compounds (**4a–4i**) against *Agrobacterium tumefaciens*-induced tumor in potato discs.

Table 2. Binding energies, dissociation constants of synthesized compounds, native ligands, and vinblastine.

Sr. No.	Compound	Protein	Binding Energy (kcal/mol)	Dissociation Constant (nM)	Main Contacting Amino Acid Residues
1	4a	CDK-8	-9.22	175.54	Lys-47, Asp-98, Gly-161 & Glu-101
2	4b		-8.45	89.46	Lys-47, Tyr-99, Gly-161 & Glu-101
3	4c		-9.41	444.39	His-154, Pro-194 & Phe-195,
4	4d		-8.87	194.89	Lys-47, Asp-48, Tyr-99, & Gly-161

Table 2. Cont.

Sr. No.	Compound	Protein	Binding Energy (kcal/mol)	Dissociation Constant (nM)	Main Contacting Amino Acid Residues
5	4e		−9.33	192.9	Lys-47, Tyr-99, Gly-161 & Glu-165
6	4f		−8.66	83.5	Tyr-153, Tyr-156, Arg-157 & Pro-158
7	4g		−9.53	106.69	Lys-47, Asp-98, Tyr-99 & Glu-101
8	4h		−9.52	104.28	Trp-6, Glu-98, His-154 & Pro-194
9	4i		−8.53	98.42	Phe-5, Glu-98, His-154 & Phe-195
10	Vinblastine		−9.11	3170	Asp-46, Lys-47, Gly-161 & Lys-355
11	5XG		−9.18	185.8	Val-27, Ala-100, Asp-173 & Arg-356

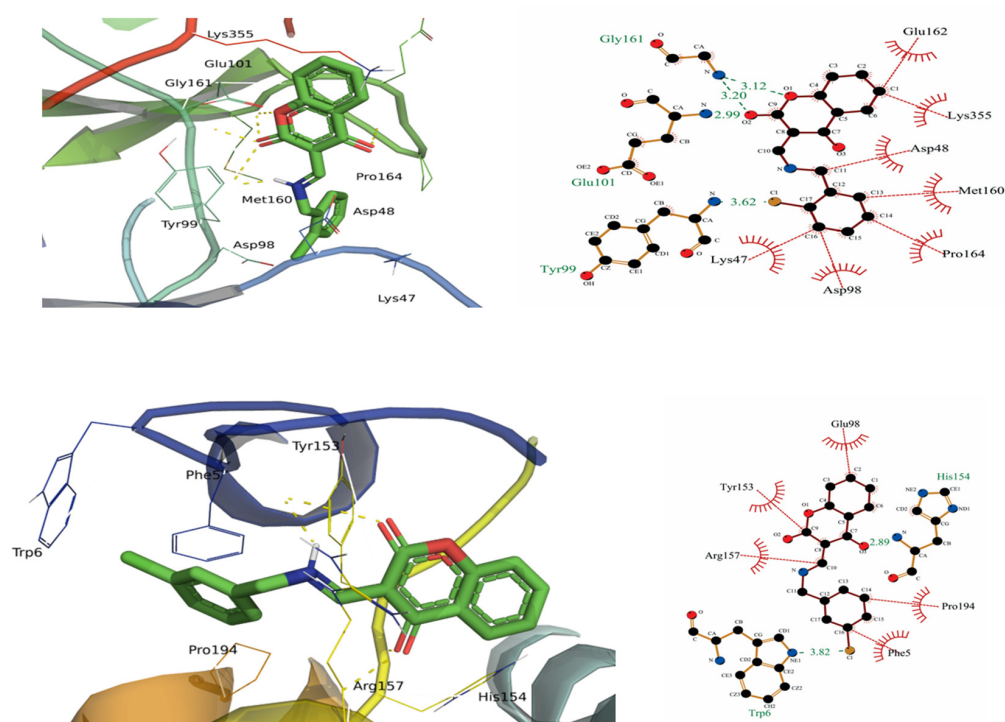


Figure 4. Docking simulation of the interaction between compounds (4g and 4h) and CDK-8.

3. Experimental Section

3.1. Materials and Methods

Analytical grade chemicals purchased from Merck and Sigma Aldrich (Darmstadt, Germany) were used without further purification. Solvents were used in raw form for a solubility check. Melting points were determined using the Fisher-Johns melting point apparatus (Thermo Scientific, Waltham, MA, USA). Spectrophotometer (SHIMADZU UV 240, Kyoto, Japan) and FT-IR (Shimadzu Prestige-21, Kyoto, Japan) were used to record UV/Visible and FTIR spectra, respectively. Nuclear magnetic resonance spectra were recorded in DMSO- d_6 on Bruker AM 300 spectrometer (Rhenistetten-Forchheim, Germany) operating at 300 MHz and using TMS as an internal standard. The chemical shifts (δ) are reported in parts per million (ppm) and coupling constants in Hz.

3.2. Synthesis of Substituted 3-((Benzylamino)methylene)-3H-chromene-2,4-dione (4a–4i)

Synthesis of substituted 3-((benzylamino)methylene)-3H-chromene-2,4-dione is reported following the literature [37–39] with slight modification. A total of 2.5 mmol of substituted benzylamine (2) in 2-butanol was added dropwise in an equimolar solution of 4-hydroxycoumarin (1) in the same solvent, with a slight excess of ethyl orthoformate under reflux conditions. The progress of the reaction was continuously monitored by TLC.

After 3–4 h reflux, the product precipitates adhered to the flask surfaces, indicating the completion of the reaction. Precipitates were filtered, washed with ethanol, dried in an oven, and stored in airtight bottles as a purified product. Figure 5 represents the general scheme of synthesis and structures of compounds (4a–4i).

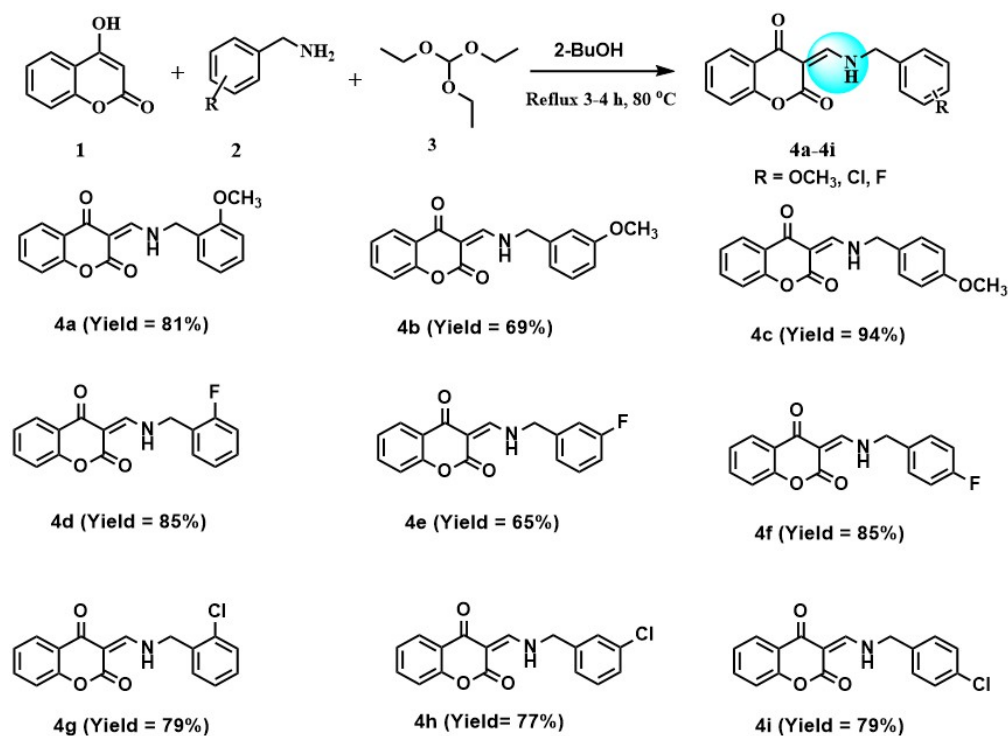


Figure 5. General scheme of synthesis and structures of 3-formyl-4-hydroxycoumarin-based enamines (4a–4i).

3-((2-methoxybenzylamino)methylene)-3H-chromene-2,4-dione (4a)

Yield: 81%; pink crystalline solid; FTIR (KBr, cm^{-1}): 3380 (N-H), 1690 (C=O), 1626 (C=C); λ_{max} (cm^{-1}): 19,495; $^1\text{H-NMR}$: (300 MHz, DMSO-d_6) δ (ppm): 3.94 (s, OCH₃) 4.66 (d, $J = 6.0$ Hz, 2H, CH₂ (E)); 4.70 (d, $J = 6.0$ Hz, 2H, CH₂ (Z)), 6.95 (dd, $J = 9.0$ Hz & $J = 6.0$ Hz, 2H, Ph, Ar-H & Ar-H), 7.00–7.28(m, 2H, Ar-H), 7.34–7.40 (m, 2H, Ar-H), 7.53–7.56 (m, 1H, Ar-H), 8.00 (dd $J_{5,6} = 6.0$ Hz, $J_{5,7} = 3.0$ Hz, 1H, Ar-H (E)), 8.02 (dd $J_{5,6} = 6.0$ Hz, $J_{5,7} = 3.0$ Hz, 1H, Ar-H(Z)), 8.52 (d, $J_{\text{H(9),NH}} = 12$ Hz, C₉-H (E)), 8.65 (d, $J_{\text{H(9),NH}} = 12$ Hz, C₉-H(Z)); 10.62 (s, br, 1H, NH (Z)), 12.07 (s, br, 1H, NH, (E)) (Figure S1A); $^{13}\text{C-NMR}$ (300 MHz, CDCl_3) 51.21, 55.54, 110.86, 117.24, 120.92, 122.90, 123.85, 124.04, 125.64, 126.35, 129.68, 130.55, 134.12, 157.58, 160.50, 162.14 (Figure S1B); EI-MS, m/z (%): 309(M^+ ,100), 294(7.1), 278(3.6), 249(1.5), 188(12.5), 176(7.1), 147(1.8), 134(5.6), 121(64.8), 91(59.8), 82.9(26.8), 65(7.1), 51(2.4), 44(19.0); elemental analysis: C₁₈H₁₅NO₄: (309.32); calculated (%): C; 69.89, H; 4.89, N; 4.53; found (%): C; 69.90, H; 4.85, N; 4.53; melting point: 218 °C.

3-((3-methoxybenzylamino)methylene)-3H-chromene-2,4-dione (4b)

Yield: 69%; Pink amorphous solid; FTIR (KBr, cm^{-1}): 3400 (N-H), 1701 (C=O), 1647 (C=C); λ_{max} (cm^{-1}): 19,435; $^1\text{H-NMR}$: (300 MHz, DMSO-d_6) δ (ppm): 3.82 (s, OCH₃), 4.68 (d, $J = 6.0$ Hz, 2H, CH₂ (E)), 4.72 (d, $J = 6.0$ Hz, 2H, CH₂ (Z)), 6.83 (t, $J = 3.0$ Hz, 1H, ph, C₂'-H), 6.88–6.93 (m, 2H, Ar-H), 7.24–7.33 (m, 1H, Ar-H), 8.00 (dd $J_{5,6} = 6.0$ Hz, $J_{5,7} = 3.0$ Hz, 1H, C₅-H (E)), 8.02 (dd $J_{5,6} = 6.0$ Hz, $J_{5,7} = 3.0$ Hz, 1H, Ar-H (Z)), 8.50 (d, $J_{\text{H(9),NH}} = 15$ Hz, C₉-H (E)), 8.66 (d, $J_{\text{H(9),NH}} = 15$ Hz, C₉-H (Z)), 10.48 (s Br, 1H, NH (Z)), 12.14 (s, br, 1H, NH (E)) (Figure S2A); $^{13}\text{C-NMR}$ (300 MHz, CDCl_3); 55.44, 54.57, 97.35, 113.53, 114.13, 117.32, 119.87, 120.53, 123.99, 124.20, 130.44, 134.39, 135.95, 160.27, 160.68, 162.24 (Figure S2B); EI-MS, m/z (%): 309(M^+ ,100), 294(12), 292(22.9), 279(5.1), 249(3.2), 188(29.7), 176(8.8), 172(65.9), 160(12.5), 147(8.7), 134(12.7), 121(58.9), 91(18), 65(6.4), 51(2.7), 44(9.2).; elemental

analysis: $C_{18}H_{15}NO_4$: (309.32); calculated (%): C; 69.89, H; 4.89, N; 4.53; found (%): C; 69.90, H; 4.85, N; 4.53; melting point: 118 °C.

3-((4-methoxybenzylamino)methylene)-3H-chromene-2,4-dione (4c)

Yield: 94%; Pink amorphous solid; FTIR (KBr, cm^{-1}): 3400 (N-H), 1705 (C=O), 1607 (C=C); λ_{max} (cm^{-1}): 19,460; 1H -NMR: (300 MHz, DMSO- d_6) δ (ppm): 3.83 (s, OCH₃), 4.65 (d, $J = 6.0$ Hz, 2H, CH₂ (E)), 4.68 (d, $J = 6.0$ Hz, 2H, CH₂ (Z)), 6.93 (d, $J = 3.0$ Hz, 2H, Ar-H), 7.23–7.28 (m, 4 H, Ar-H), 7.55–7.58 (m, 1H, Ar-H), 8.00 (dd $J_{5,6} = 6.0$ Hz, $J_{5,7} = 3.0$ Hz, 1H, Ar-H (E)), 8.02 (dd $J_{5,6} = 6.0$ Hz, $J_{5,7} = 3.0$ Hz, 1H, Ar-H (Z)), 8.48 (d, $J_{H(9),NH} = 15$ Hz, C₉-H (E)), 8.64 (d, $J_{H(9),NH} = 15$ Hz, C₉-H (Z)), 10.44 (s, br, 1H, NH (Z)), 12.11 (s, br, 1H, NH, (E)) (Figure S3A); ^{13}C -NMR (300 MHz, CDCl₃): 54.05, 54.14, 55.38, 99.99, 114.72, 117.30, 123.97, 124.17, 125.68, 126.29, 126.40, 129.32, 134.33, 160.29, 161.86 (Figure S3B); EI-MS, m/z (%): 309(89.5), 292(7.1), 280(1.5), 188(5.7), 176(4.0), 172(7.5), 160(2.8), 147(1.6), 134(5.2), 121(M^+ 100), 91(3.7), 63(2.5), 51(1.7), 44(14.3); elemental analysis: $C_{18}H_{15}NO_4$: (309.32); calculated (%): C; 69.89, H; 4.89, N; 4.53; found (%): C; 69.90, H; 4.85, N; 4.53; melting point: 182 °C.

3-((2-fluorobenzylamino)methylene)-3H-chromene-2,4-dione (4d)

Yield: 85%; Light pink amorphous solid; FTIR (KBr, cm^{-1}): 3220 (N-H), 1713 (C=O), 1634 (C=C); λ_{max} (cm^{-1}): 19,390; 1H -NMR: (300 MHz, DMSO- d_6) δ (ppm): 4.75 (d, $J = 6.0$ Hz, 2H, CH₂ (E)), 4.79 (d, $J = 6.0$ Hz, 2H, CH₂ (Z)), 7.15–7.39 (m, 2H, Ar-H), 7.55–7.58 (m, 4 H, Ar-H), 7.55–7.58 (m, 1H, Ar-H), 8.01 (dd $J_{5,6} = 6.0$, $J_{5,7} = 3.0$ Hz, 1H, Ar-H (E)), 8.02 (dd $J_{5,6} = 6.0$, $J_{5,7} = 3.0$ Hz, 1H, C₅-H (Z)), 8.53 (d, $J_{H(9),NH} = 15$ Hz, C₉-H (E)), 8.68 (d, $J_{H(9),NH} = 15$ Hz, C₉-H (Z)), 10.46 (s, br, 1H, NH (Z)), 12.15 (s, br, 1H, NH (E)) (Figure S4A); ^{13}C -NMR (300 MHz, CDCl₃): 48.86, 48.91, 115.98, 116.26, 117.32, 124.00, 124.88, 124.93, 125.71, 126.44, 129.83, 129.88, 131.00, 131.11, 134.44, 160.84, 162.43 (Figure S4B); EI-MS, m/z (%): 297(M^+ 100), 280(10.7), 268(2.4), 252(1.8), 203(3.3), 188(87.5), 176(25.6), 160(16.2), 148.1(10.2), 135(2.2), 121(36.4), 109(94.3), 92(5.6), 82.9(19.7), 63(7.5), 51(2.9), 44(9.5); elemental analysis: $C_{17}H_{12}NO_3F$: (297.30); calculated (%): C; 68.68, H; 4.07, N; 4.71; found (%): C; 68.69, H; 4.04, N; 4.71; melting point: 140 °C.

3-((3-fluorobenzylamino)methylene)-3H-chromene-2,4-dione (4e)

Yield: 65%, Light pink crystalline solid; FTIR (KBr, cm^{-1}): 3215 (N-H), 1701 (C=O), 1632 (C=C); λ_{max} (cm^{-1}): 19,480; 1H -NMR: (300 MHz, DMSO- d_6) δ (ppm): 4.71 (d, $J = 6.0$ Hz, 2H, CH₂ (E)), 4.75 (d, $J = 6.0$ Hz, 2H, CH₂ (Z)), 7.04 (d, $J = 9.0$ Hz, 2H, Ar-H), 7.07 (d, $J = 6.0$ Hz, 1H, Ar-H), 7.09–7.41 (m, 2H, Ar-H), 7.56–7.59 (m, 1H, Ar-H), 7.59–7.61 (m, 1H, Ar-H), 8.01 (dd $J_{5,6} = 6.0$ Hz, $J_{5,7} = 3.0$ Hz, 1H, C₅-H (E)), 8.02 (dd $J_{5,6} = 6.0$ Hz, $J_{5,7} = 3.0$ Hz, 1H, Ar-H (Z)), 8.53 (d, $J_{H(9),NH} = 15$ Hz, C₉-H (E)), 8.68 (d, $J_{H(9),NH} = 15$ Hz, C₉-H (Z)), 10.50 (s, br, 1H, NH (Z)), 12.16 (s, br, 1H, NH (E)) (Figure S5A); ^{13}C -NMR (300 MHz, CDCl₃): 53.83, 53.96, 97.56, 114.57, 114.86, 115.74, 116.02, 117.30, 117.35, 120.45, 123.18, 123.22, 124.06, 124.27, 125.73, 129.83, 125.73, 126.43, 130.96, 131.07, 134.53, 136.98, 154.93, 160.85, 162.44 (Figure S5B); EI-MS, m/z (%): 293(M^+ 100), 280(20.8), 268(3.2), 252(3.0), 203(2.9), 188(67.1), 176(24.3), 160(41), 148.1(12.7), 135(4.9), 121(39.9), 109(63.5), 92(5.9), 82.9(44.2), 63(5.5), 51(2.7), 44(8.4); elemental analysis: $C_{17}H_{12}NO_3F$: (297.30); calculated (%): C; 68.68, H; 4.07, N; 4.71; found (%): C; 68.69, H; 4.04, N; 4.71; melting point: 180 °C.

3-((4-fluorobenzylamino)methylene)-3H-chromene-2,4-dione (4f)

Yield: 85%; Light pink crystalline solid; FTIR (KBr, cm^{-1}): 3050 (N-H), 1715 (C=O), 1638 (C=C); λ_{max} (cm^{-1}): 19,450; 1H -NMR: (300 MHz, DMSO- d_6) δ (ppm): 4.71 (d, $J = 6.0$ Hz, 2H, CH₂ (E)), 4.75 (d, $J = 6.0$ Hz, 2H, CH₂ (Z)); 7.09 (d, $J = 9.0$ Hz 2H, Ar-H), 7.33–7.56 (m, 4H, Ar-H), 7.56–7.58 (m, 1H, Ar-H), 8.01 (dd $J_{5,6} = 6.0$ Hz, $J_{5,7} = 3.0$ Hz, 1H, Ar-H (E)), 8.02 (dd $J_{5,6} = 6.0$ Hz, $J_{5,7} = 3.0$ Hz, 1H, Ar-H (Z)), 8.50 (d, $J_{H(9),NH} = 15$ Hz, C₉-H (E)), 8.71 (d, $J_{H(9),NH} = 15$ Hz, C₉-H (Z)), 10.46 (s, br, 1H, NH (Z)), 12.13 (s, br, 1H, NH, (E)) (Figure S6A); ^{13}C -NMR (300 MHz, CDCl₃): 53.77, 53.89, 97.42, 116.21, 116.50, 116.70, 117.34, 124.05, 124.45, 124.81, 125.71, 126.43, 129.57, 132.56, 134.49, 160.58, 162.16, 164.56. EI-MS, m/z (%): 297(M^+ 100), 280(11.3), 268(2.0), 252(1.4), 203(1.6), 188(34), 176(15.3), 160(17.7), 148.1(7.1), 135(2.2), 121(21.4), 109(92.2), 92(3.4), 63(4.9), 51(1.8), 44(16.5) (Figure S6B); elemental analysis: $C_{17}H_{12}NO_3F$: (297.30); calculated (%): C; 68.68, H; 4.07, N; 4.71; found (%): C; 68.69, H; 4.04, N; 4.71; melting point: 175 °C.

3-((2-chlorobenzylamino)methylene)-3H-chromene-2,4-dione (4g)

Yield: 79%; Pink amorphous solid; FTIR (KBr, cm^{-1}): 3250 (N-H), 1726 (C=O), 1655 (C=C); λ_{max} (cm^{-1}): 19,410; $^1\text{H-NMR}$ (300 MHz, DMSO- d_6) δ (ppm): 4.80 (d, $J = 6.0$ Hz, 2H, CH_2 (E)), 4.84 (d, $J = 6.0$ Hz, 2H, CH_2 (Z)), 7.23–7.36 (m, 2H, Ar-H), 7.38–3.55 (m, 3H, Ar-H), 7.57–7.58 (m, 1H, Ar-H), 7.58 (m, 1H, Ar-H), 8.01 (dd $J_{5,6} = 9.0$ Hz, $J_{5,7} = 3.0$ Hz, 1H, Ar-H (E)), 8.04 (dd $J_{5,6} = 9.0$ Hz, $J_{5,7} = 3.0$ Hz, 1H, Ar-H (Z)), 8.52 (d, $J_{\text{H(9),NH}} = 12$ Hz, $\text{C}_9\text{-H}$ (E)), 8.67 (d, $J_{\text{H(9),NH}} = 15$ Hz, $\text{C}_9\text{-H}$ (Z)), 10.50 (s, br, 1H, NH (Z)), 12.19 (s, br, 1H, NH (E)) (Figure S7A); $^{13}\text{C-NMR}$ (300 MHz, CDCl_3): 52.45, 52.67, 97.49, 117.32, 120.50, 124.01, 124.21, 125.73, 126.43, 127.68, 129.95, 130.24, 130.49, 132.40, 134.44, 154.92, 160.95, 162.52 (Figure S7B); EI-MS, m/z (%): 313($\text{M}^+ 100$), 296(4.1), 278(11.0), 257(8.9), 249(2.3), 188(7.1), 176(18.4), 158(5.6), 140(9.9), 125(38.7), 89(5.6), 63(7.3), 44(29.2); elemental analysis: $\text{C}_{17}\text{H}_{12}\text{NO}_3\text{Cl}$: (313.74); calculated (%): C; 65.08, H; 3.86, N; 4.46; found (%): C; 65.07, H; 3.83, N; 4.46; melting point: 165 °C.

3-((3-chlorobenzylamino)methylene)-3H-chromene-2,4-dione (4h)

Yield: 77%; Light purple crystalline solid; FTIR (KBr, cm^{-1}): 3233 (N-H), 1703 (C=O), 1630 (C=C); λ_{max} (cm^{-1}): 19,550; $^1\text{H-NMR}$: (300 MHz, DMSO- d_6) δ (ppm): 4.69 (d, $J = 6.0$ Hz, 2H, CH_2 (E), 4.74 (d, $J = 9.0$ Hz, 2H, CH_2 (Z)), 7.20–7.37 (m, 2H, Ar-H), 7.56–7.59 (m, 4 H, Ar-H), 7.59 (m, 1H, Ar-H), 8.01 (dd $J_{5,6} = 6.0$ Hz, $J_{5,7} = 3.0$ Hz, 1H, Ar-H (E)), 8.03 (dd $J_{5,6} = 6.0$ Hz, $J_{5,7} = 3.0$ Hz, 1H, Ar-H (Z)), 8.51 (d, $J_{\text{H(9),NH}} = 15$ Hz, $\text{C}_9\text{-H}$ (E)), 8.66 (d, $J_{\text{H(9),NH}} = 15$ Hz, $\text{C}_9\text{-H}$ (Z)), 10.48 (s, br, 1H, NH (Z)), 12.15 (s, br, 1H, NH (E)) (Figure S8A); $^{13}\text{C-NMR}$ (300 MHz, CDCl_3): 53.80, 53.96, 117.31, 117.36, 120.45, 124.07, 124.28, 125.73, 126.44, 127.84, 129.09, 130.61, 134.55, 136.58, 154.93, 160.83, 162.42 (Figure S8A); EI-MS, m/z (%): 293($\text{M}^+ 100$), 296(15.5), 278(26.2), 249(1.6), 219(2.6), 188(68.9), 176(54.4), 164(7.7), 146(4.6), 139(7.6), 125(48.4), 105(1.9), 82.9(28.5), 89(11.1), 63(6.4), 44(14.4); elemental analysis: $\text{C}_{17}\text{H}_{12}\text{NO}_3\text{Cl}$: (313.74); calculated (%): C; 65.08, H; 3.86, N; 4.46; found (%): C; 65.07, H; 3.83, N; 4.46; melting point: 176 °C.

3-((4-chlorobenzylamino)methylene)-3H-chromene-2,4-dione (4i)

Yield: 79%; Light pink crystalline solid; FTIR (KBr, cm^{-1}): 3200 (N-H), 1715 (C=O), 1636 (C=C); λ_{max} (cm^{-1}): 19,608; $^1\text{H-NMR}$ (300 MHz, DMSO- d_6) δ (ppm): 4.71(d, $J = 6.0$ Hz, 2H, CH_2 (E)), 4.73 (d, $J = 9.0$ Hz, 2H, CH_2 (Z)), 7.23–7.42 (m, 4 H, ph), 7.56–7.59 (m, 2H, $\text{C}_6\text{-H}$ & $\text{C}_8\text{-H}$), 7.61 (m, 1H, $\text{C}_7\text{-H}$), 8.00 (dd $J_{5,6} = 6.0$ Hz, $J_{5,7} = 3.0$ Hz, 1H, $\text{C}_5\text{-H}$ (E)), 8.02 (dd $J_{5,6} = 6.0$ Hz, $J_{5,7} = 3.0$ Hz, 1H, $\text{C}_5\text{-H}$ (Z)), 8.50 (d, $J_{\text{H(9),NH}} = 15$ Hz, $\text{C}_9\text{-H}$ (E)), 8.65 (d, $J_{\text{H(9),NH}} = 12$ Hz, $\text{C}_9\text{-H}$ (Z)), 10.47 (s (br.), 1H, NH (Z)), 12.14 (s (br.), 1H, NH (E)) (Figure S9A); $^{13}\text{C-NMR}$ (300 MHz, CDCl_3): 53.75, 53.88, 97.51, 117.35, 120.45, 124.07, 124.28, 125.73, 126.43, 129.05, 129.53, 133.05, 134.53, 160.71, 162.30 (Figure S9B); EI-MS, m/z (%): 313($\text{M}^+ 100$), 296(13.8), 278(2.1), 219(1.7), 188(43.5), 176(32.4), 164(5.0), 146(3.4), 138(6.8), 125(81.7), 105(1.8), 89(9.6), 63(4.6), 51(2.5), 44(9.7); elemental analysis: $\text{C}_{17}\text{H}_{12}\text{NO}_3\text{Cl}$: (313.74); calculated (%): C; 65.08, H; 3.86, N; 4.46; found (%): C; 65.07, H; 3.83, N; 4.46; melting point: 166 °C.

3.3. Proposed Mechanism of Reaction

For insight into the chemical reaction, a mechanism was proposed to form the targeted product, as shown in Figure 6 [27]. Briefly, in the first step, the nucleophilic addition of benzylamine (I) to triethyl orthoformate (II) occurs, releasing two molecules of ethanol. In the second step, the imine intermediate (III) reacts with a molecule of 4-hydroxycoumarin to produce aminal (IV). In the third and final step, another ethanol molecule is eliminated from aminal (IV), forming the final product, enamine (V).

3.4. Potato Disc Tumor Assay

Agrobacterium tumefaciens was kept in nutrient agar for 48 h before use in the assay. *A. tumefaciens* were standardized to 1×10^9 CFU in phosphate-buffered saline. Fresh potatoes purchased from the local market of Sargodha, Pakistan, were washed several times with distilled water and bleach to remove impurities on the surface. The potato skin was peeled off after cleaning the surface with a sterile towel. After peeling, potatoes were

washed with distilled water and cut into small discs of 0.5 cm in diameter. These discs were placed in a 24-well culture plate containing 15% agar in water. Dilute solutions of the as-synthesized compounds containing both the isomers ('E' and 'Z' isomer) (4a–4i) in the range of 0.1–50 mg/mL were prepared in DMSO and 50 μ L of each solution was applied on potato disc. Pure DMSO was used as a negative control, and vinblastine (standard drug) solutions in DMSO were used as a positive control. Vinblastine was used as a positive control due to its almost similar mode of action as the synthesized compounds (4a–4i); it binds to the microtubular proteins to hinder the cell division of cancer cells [35]. After incubation for 14 days, discs were stained with Lugol's reagent. This reagent stained the starch in the discs to blue, but the tumors appeared creamy. Tumors were counted under a microscope in each disc to calculate the IC₅₀ values.

The bacterial viability of compounds was also checked by the disc diffusion method by loading sterile paper discs with compounds (0.1 mg/mL). Pure DMSO was used as a positive control. After incubation of 48 h, the growth of bacteria was evident, which showed the non-active nature of the compounds at this concentration (0.1 mg/mL) toward bacteria.

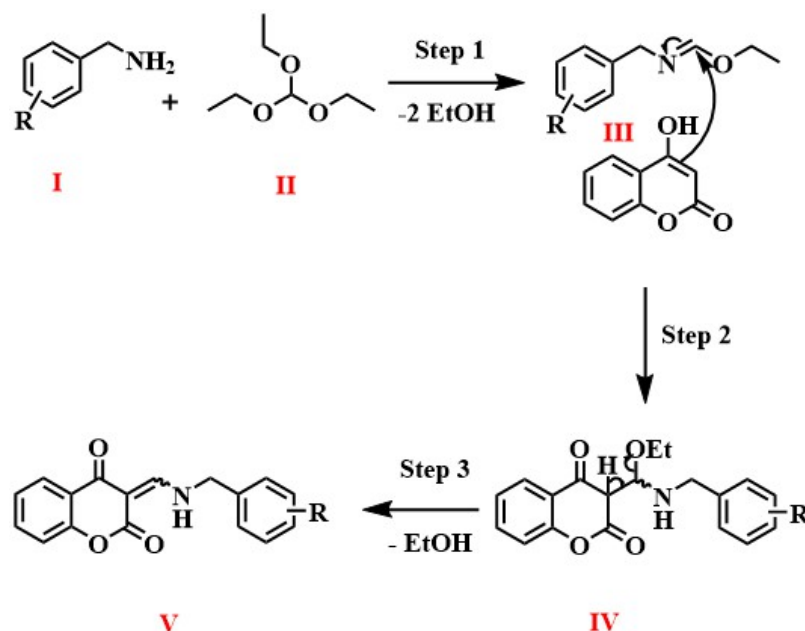


Figure 6. Proposed mechanism for the synthesis of enamines from 4-hydroxycoumarin. Benzylamine (I), triethyl orthoformate (II) the imine intermediate (III), aminor (IV), enamine (V).

3.5. Molecular Docking Analysis

The *in silico* anti-tumor activity of synthesized compounds was predicted by screening against the CDK-8 protein using a YASARA (Yet Another Scientific Artificial Real Application) software version 20.7.4 [40]. The 3D structure of CDK-8, as shown in Figure 7, was obtained from Protein Data Bank (PDB ID, 5FGK). AutoDock LGA module and AMBER03 forcefields in YASARA with 100 global docking runs and 1000 random seed values were used for docking. The AutoDock local search (LGA-LS) method in YASARA was then used to rescore docked ligands (4a–4i), as described before [41].

The docking scoring and rescoring were calculated following the empirical Equation (1).

$$\Delta G = \Delta G_{(\text{Van der Waal})} + \Delta G_{(\text{H-bonding})} + \Delta G_{(\text{electrostatic})} + \Delta G_{(\text{torsional free energy})} + \Delta G_{(\text{desolvation energy})} \quad (1)$$

The LigPlus [42] and PyMOL [43] were used to extract the lowest energy binding energy docking poses, and ligand-protein interactions were mapped.

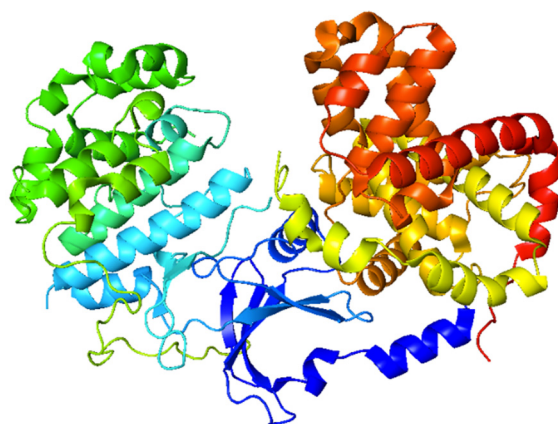


Figure 7. Crystal structure of CDK-8 enzyme.

3.6. Statistical Analysis

Each bioactivity experiment was repeated thrice, and results were analyzed statistically by ANOVA. Statistical significance was accepted at a level of $p < 0.05$. Mean \pm SD values were reported in tables and graphs.

4. Conclusions

Novel 3-formyl-4-hydroxycoumarin-derived enamines (**4a–4i**) were synthesized by a one-pot condensation reaction and characterized by state-of-the-art spectroscopic and analytical techniques. All the compounds were evaluated for their anti-tumor potential against *Agrobacterium tumefaciens* by potato disc tumor assay. The bacterial viability of compounds was also checked, which showed no prominent effect on bacterial growth. Five compounds (**4a**, **4c**, **4e**, **4g**, and **4h**) have shown better activity than the standard drug, vinblastine. Molecular docking simulations of compounds were also performed with the human protein CDK-8. This enzyme is actively involved in the cell cycle, and the synthesized compounds have shown good binding affinities with this protein. Molecular docking results were in good agreement with the experimental IC_{50} values of the compounds.

Supplementary Materials: The following supporting information can be downloaded at: <https://www.mdpi.com/article/10.3390/molecules28155828/s1>, Potato disc assay results, 1H -NMR spectra, ^{13}C -NMR spectra and molecular docking diagrams are given in supporting information.

Author Contributions: M.A.: Data curation, anti-tumor studies, writing—original draft preparation; R.N.P.: methodology, conceptualization, writing—reviewing and editing; A.B.S., M.M. and C.L.: conceptualization, data curation, writing—original draft preparation; M.A.S.: conceptualization, data curation, writing—original draft preparation; N.A. and F.K.: data curation, methodology, software; M.F.u.R. and S.F.: data curation, molecular docking studies, writing—original draft; M.Z.U.M.: visualization, writing—original draft preparation. All authors have read and agreed to the published version of the manuscript.

Funding: Funding in the C.L. lab was provided by the Fundamental Research Funds for the Central Universities (2232021G-04), Shanghai Science and Technology Committee (19ZR1471100). The authors are also thankful for the online utilization of computational resources at C.L. lab, Donghua University, China.

Data Availability Statement: The raw spectra and data are available on request.

Acknowledgments: The authors extend their appreciation to the Researchers group of Changrui Lu for financial support of this project.

Conflicts of Interest: The authors declare that they have no known competing financial interest or personal relationships that could have appeared to influence the work reported in this paper.

Sample Availability: Sample of the compounds are available from authors on request.

References

1. Huang, Q.; Wang, X.; Chen, A.; Zhang, H.; Yu, Q.; Shen, C.; Awadasseid, A.; Zhao, X.; Xiong, X.; Wu, Y.; et al. Design, synthesis and anti-tumor activity of novel benzothiofenonaphthalimide derivatives targeting mitochondrial DNA (mtDNA) G-quadruplex. *Biochem. Pharmacol.* **2022**, *201*, 115062. [[CrossRef](#)] [[PubMed](#)]
2. McGuire, S. World cancer report 2014. Geneva, Switzerland: World Health Organization, international agency for research on cancer, WHO Press, 2015. *Adv. Nutr.* **2016**, *7*, 418–419. [[CrossRef](#)] [[PubMed](#)]
3. Nagai, H.; Kim, Y.H. Cancer prevention from the perspective of global cancer burden patterns. *J. Thorac. Dis.* **2017**, *9*, 448. [[CrossRef](#)]
4. Subramanian, A.; John, A.; Vellayappan, M.; Balaji, A.; Jaganathan, S.; Supriyanto, E.; Yusof, M. Gallic acid: Prospects and molecular mechanisms of its anticancer activity. *RSC Adv.* **2015**, *5*, 35608–35621. [[CrossRef](#)]
5. Zaki, M.; Hairat, S.; Aazam, E.S. Scope of organometallic compounds based on transition metal-arene systems as anticancer agents: Starting from the classical paradigm to targeting multiple strategies. *RSC Adv.* **2019**, *9*, 3239–3278. [[CrossRef](#)]
6. Lv, W.; Fu, B.; Li, M.; Kang, Y.; Bai, S.; Lu, C. Determination of IC 50 values of anticancer drugs on cells by D₂O–single cell Raman spectroscopy. *Chem. Comm.* **2022**, *58*, 2355–2358. [[CrossRef](#)]
7. Suroowan, S.; Mahomoodally, M.F. Tradition Meets Innovation: Herbal Medicine as a Sustainable Source of Anticancer Agents. In *Urban Health Risk and Resilience in Asian Cities*; Springer: Berlin/Heidelberg, Germany, 2020; pp. 367–387.
8. Boros, E.; Dyson, P.J.; Gasser, G. Classification of metal-based drugs according to their mechanisms of action. *Chem* **2020**, *6*, 41–60. [[CrossRef](#)]
9. Gailer, J. Improving the safety of metal-based drugs by tuning their metabolism with chemoprotective agents. *J. Inorg. Biochem.* **2018**, *179*, 154–157. [[CrossRef](#)]
10. Vaseghi, S.; Yousefi, M.; Shokrzadeh, M.; Hossaini, Z.; Hosseini-Khah, Z.; Emami, S. Synthesis, computational study and cytotoxicity of 4-hydroxycoumarin-derived imines/enamines. *Mol. Divers.* **2021**, *25*, 1011–1024. [[CrossRef](#)]
11. Ibrahim, M.; Latif, A.; Ahmad, M.; Ahmad, S.; Ali, A.; Siddique, A.B.; Saadiq, M.; Akbar, N.; Khan, A.; Al-Harrasi, A. Sulfonylbis (acylhydrazones) as anticholinesterase inhibitors: Synthesis, in vitro biological evaluation and computational studies. *J. Mol. Struct.* **2022**, *1252*, 132215. [[CrossRef](#)]
12. Malik, A.N.; Kuznetsov, A.; Ali, A.; Ashfaq, M.; Tahir, M.N.; Siddique, A. Imine-based Zwitterion: Synthesis, single-crystal characterization, and computational investigation. *J. Mol. Struct.* **2022**, *1253*, 132237. [[CrossRef](#)]
13. Uroos, M.; Javaid, A.; Bashir, A.; Tariq, J.; Khan, I.H.; Naz, S.; Fatima, S.; Sultan, M. Green synthesis of coumarin derivatives using Brønsted acidic pyridinium based ionic liquid [MBSPy][HSO₄] to control an opportunistic human and a devastating plant pathogenic fungus *Macrophomina phaseolina*. *RSC Adv.* **2022**, *12*, 23963–23972. [[CrossRef](#)] [[PubMed](#)]
14. Sharifi-Rad, J.; Cruz-Martins, N.; López-Jornet, P.; Lopez, E.P.-F.; Harun, N.; Yeskaliyeva, B.; Beyatli, A.; Sytar, O.; Shaheen, S.; Sharopov, F. Natural coumarins: Exploring the pharmacological complexity and underlying molecular mechanisms. *Oxid. Med. Cell. Longev.* **2021**, *2021*, 6492346. [[CrossRef](#)] [[PubMed](#)]
15. Garg, S.S.; Gupta, J.; Sharma, S.; Sahu, D. An insight into the therapeutic applications of coumarin compounds and their mechanisms of action. *Eur. J. Pharm. Sci.* **2020**, *152*, 105424. [[CrossRef](#)] [[PubMed](#)]
16. Song, J.; Ham, J.; Hong, T.; Song, G.; Lim, W. Fraxetin suppresses cell proliferation and induces apoptosis through mitochondria dysfunction in human hepatocellular carcinoma cell lines Huh7 and Hep3B. *Pharmaceutics* **2021**, *13*, 112. [[CrossRef](#)]
17. Konarska-Bajda, K.; Ceranowicz, P.; Cieszkowski, J.; Ginter, G.; Stempniewicz, A.; Gałazka, K.; Warzecha, Z. Administration of Warfarin Inhibits the Development of Cerulein-Induced Edematous Acute Pancreatitis in Rats. *Biomolecules* **2023**, *13*, 948. [[CrossRef](#)]
18. Tossetta, G.; Fantone, S.; Goteri, G.; Giannubilo, S.R.; Ciavattini, A.; Marzioni, D. The Role of NQO1 in Ovarian Cancer. *Int. J. Mol. Sci.* **2023**, *24*, 7839. [[CrossRef](#)]
19. Ma, Z.; Peng, L.; Chu, W.; Wang, P.; Fu, Y. Osthole Alleviates D-Galactose-Induced Liver Injury In Vivo via the TLR4/MAPK/NF-κB Pathways. *Molecules* **2023**, *28*, 443. [[CrossRef](#)]
20. Youness, R.A.; Al-Mahallawi, A.M.; Mahmoud, F.H.; Atta, H.; Braoudaki, M.; Fahmy, S.A. Oral Delivery of Psoralidin by Mucoadhesive Surface-Modified Bilosomes Showed Boosted Apoptotic and Necrotic Effects against Breast and Lung Cancer Cells. *Polymers* **2023**, *15*, 1464. [[CrossRef](#)]
21. Magoo, D.; Aggarwal, K.; Gupta, S.; Meena, K. Enamines and their variants as intermediates for synthesis of aza-heterocycles with applications in MCRs. *Tetrahedron* **2022**, *103*, 132545. [[CrossRef](#)]
22. Vodolazhenko, M.A.; Gorobets, N.Y.; Zhikol, O.A.; Desenko, S.M.; Shishkin, O.V. A quantum chemical approach towards understanding stability and tautomerism of 2-imino-2H-pyran derivatives. *RSC Adv.* **2016**, *6*, 52201–52211. [[CrossRef](#)]
23. Farid, S.M.; Seifinoferest, B.; Gholamhosseini, M.; Larijani, B.; Mahdavi, M. Modern metal-catalyzed and organocatalytic methods for synthesis of coumarin derivatives: A review. *Org. Biomol. Chem.* **2022**, *20*, 4846–4883. [[CrossRef](#)] [[PubMed](#)]
24. Holiyachi, M.; Shastri, S.L.; Chougala, B.M.; Naik, N.S.; Pawar, V.; Shastri, L.A.; Sunagar, V.A. Design and synthesis of new series of dipyrromethane-coumarin and porphyrin-coumarin derivatives: Excellent anticancer agents. *J. Mol. Struct.* **2021**, *1237*, 130424. [[CrossRef](#)]
25. Premnath, P.N.; Craig, S.N.; Liu, S.; Anderson, E.L.; Grigoroudis, A.I.; Kontopidis, G.; McInnes, C. Iterative conversion of cyclin binding groove peptides into druglike CDK inhibitors with antitumor activity. *J. Med. Chem.* **2015**, *58*, 433–442. [[CrossRef](#)]

26. D'costa, M.; Bothe, A.; Das, S.; Kumar, S.U.; Gnanasambandan, R.; Doss, C.G.P. CDK regulators—Cell cycle progression or apoptosis—Scenarios in normal cells and cancerous cells. *Adv. Protein Chem. Struct.* **2023**, *135*, 125–177.
27. Olyaei, A.; Javarsineh, S.; Sadeghpour, M. Green synthesis and Z/E-isomerization of novel coumarin enamines induced by organic solvents. *Chem. Heterocycl. Compd.* **2018**, *54*, 934–939. [[CrossRef](#)]
28. Mpitimpiti, A.N.; Petzer, J.P.; Petzer, A.; Jordaan, J.H.; Lourens, A.C. Synthesis and evaluation of chromone derivatives as inhibitors of monoamine oxidase. *Mol. Divers.* **2019**, *23*, 897–913. [[CrossRef](#)]
29. Coker, P.; Radecke, J.; Guy, C.; Camper, N.D. Potato disc tumor induction assay: A multiple mode of drug action assay. *Phytomedicine* **2003**, *10*, 133–138. [[CrossRef](#)]
30. McLaughlin, J.L.; Hostettmann, K. Methods in plant biochemistry. *Assays Bioactivity* **1991**, *6*, 1–33.
31. Binns, A.N.; Thomashow, M.F. Cell biology of Agrobacterium infection and transformation of plants. *Annu. Rev. Microbiol.* **1988**, *42*, 575–606. [[CrossRef](#)]
32. McLaughlin, J.L.; Rogers, L.L.; Anderson, J.E. The use of biological assays to evaluate botanicals. *Drug Inf. J.* **1998**, *32*, 513–524. [[CrossRef](#)]
33. Agrwal, A.; Saini, R.; Bhandri, S.; Verma, S.; Srivastava, P.; Prakash, O. Synthesis, ADMET, drug likeness and in silico activities of benzimidazole derivative. *Mater. Today Proc.* **2022**, *67*, 598–604. [[CrossRef](#)]
34. Siddique, A.B.; Ahmad, S.; Shaheen, M.A.; Ali, A.; Tahir, M.N.; Vieira, L.C.; Muhammad, S.; Siddeeq, S.M. Synthesis, antimicrobial potential and computational studies of crystalline 4-bromo-2-(1,4,5-triphenyl-1H-imidazole-2-yl)phenol and its metal complexes. *CrystEngComm* **2022**, *24*, 8237–8247. [[CrossRef](#)]
35. Dannappel, M.V.; Sooraj, D.; Loh, J.J.; Firestein, R. Molecular and in vivo functions of the CDK8 and CDK19 kinase modules. *Front. Cell Dev. Biol.* **2019**, *6*, 171. [[CrossRef](#)]
36. Sanchez-Martinez, C.; Gelbert, L.M.; Lallena, M.J.; de Dios, A. Cyclin dependent kinase (CDK) inhibitors as anticancer drugs. *Bioorg. Med. Chem. Lett.* **2015**, *25*, 3420–3435. [[CrossRef](#)]
37. Hamdi, M.; Granier, P.; Sakellariou, R.; Spéziale, V. Reaction of amines on 3-ureidomethylenecoumarins. A new route to N-(methylene-4-oxocoumarinyl) amines. *J. Heterocycl. Chem.* **1993**, *30*, 1155–1157. [[CrossRef](#)]
38. Hamdi, M.; Sakellariou, R.; Speziale, V. New Condensation Products of Diamines with 3-Ureidomethylenecoumarin. *Org. Prep. Proced. Int.* **1995**, *27*, 487–492. [[CrossRef](#)]
39. Chun, R. Cancer Chemotherapy. In *Withrow & MacEwen's Small Animal Clinical Oncology*; Elsevier: Amsterdam, The Netherlands, 2007; pp. 163–192.
40. Krieger, E.; Vriend, G. YASARA View—Molecular graphics for all devices—From smartphones to workstations. *Bioinformatics* **2014**, *30*, 2981–2982. [[CrossRef](#)]
41. Rehman, M.F.u.; Akhter, S.; Batool, A.I.; Selamoglu, Z.; Sevindik, M.; Eman, R.; Mustaqeem, M.; Akram, M.S.; Kanwal, F.; Lu, C.; et al. Effectiveness of Natural Antioxidants against SARS-CoV-2? Insights from the In-Silico World. *Antibiotics* **2021**, *10*, 1011. [[CrossRef](#)]
42. Laskowski, R.A.; Swindells, M.B. *LigPlot+: Multiple Ligand–Protein Interaction Diagrams for Drug Discovery*; ACS Publications: Washington, DC, USA, 2011.
43. DeLano, W.L. Pymol: An open-source molecular graphics tool. *CCP4 Newsl. Protein Crystallogr.* **2002**, *40*, 82–92.

Disclaimer/Publisher's Note: The statements, opinions and data contained in all publications are solely those of the individual author(s) and contributor(s) and not of MDPI and/or the editor(s). MDPI and/or the editor(s) disclaim responsibility for any injury to people or property resulting from any ideas, methods, instructions or products referred to in the content.